Fast-Slow Analysis as a Technique for Understanding the Neuronal Response to Current Ramps

Kelsey Gasior¹, Kirill Korshunov², Paul Q. Trombley², Richard Bertram^{3*}

- ¹ Department of Mathematics, University of Ottawa, Ottawa, ON, Canada K1N 6N5
- ² Department of Biological Science and Program in Neuroscience, Florida State University, Tallahassee, FL 32306
- ³Department of Mathematics and Programs in Neuroscience and Molecular Biophysics, Florida State University, Tallahassee, FL32306
- *Corresponding Author: rbertram@fsu.edu

Email Addresses:

Kelsey Gasior: kgasior@uottawa.ca

Kirill Korshunov: kkorshunov@neuro.fsu.edu

Paul Q. Trombley: ptrombley@fsu.edu Richard Bertram: rbertram@fsu.edu

Abstract

The standard protocol for studying the spiking properties of single neurons is the application of current steps while monitoring the voltage response. Although this is informative, the jump in applied current is artificial. A more physiological input is where the applied current is ramped up. reflecting chemosensory input. Unsurprisingly, neurons can respond differently to the two protocols, since ion channel activation and inactivation are affected differently. Understanding the effects of current ramps, and changes in their slopes, is facilitated by mathematical models. However, techniques for analyzing current ramps are under-developed. In this article, we demonstrate how current ramps can be analyzed in single neuron models. The primary issue is the presence of gating variables that activate on slow time scales and are therefore far from equilibrium throughout the ramp. The use of an appropriate fast-slow analysis technique allows one to fully understand the neural response to ramps of different slopes. This study is motivated by data from olfactory bulb dopamine neurons, where both fast ramp (tens of milliseconds) and slow ramp (tens of seconds) protocols are used to understand the spiking profiles of the cells. The slow ramps generate experimental bifurcation diagrams with the applied current as a bifurcation parameter, thereby establishing asymptotic spiking activity patterns. The faster ramps elicit purely transient behavior that is of relevance to most physiological inputs, which are short in duration. The two protocols together provide a broader understanding of the neuron's spiking profile and the role that slowly activating ion channels can play.

Keywords

Multiscale system Single cell Fast-slow analysis

Declarations:

Funding

This work was supported by the FSU Chemosensory Training Program (CTP) Grant Award T32 DC000044 from the National Institutes of Health (NIH/NIDCD), NIH Grant R21DA044442 to PQT and RB, and grant number DMS 1853342 from the National Science Foundation to RB.

Conflicts of Interest

The authors declare they have no competing interests.

Availability of Data

The data sets generated for this study are available on request.

Code Availability

The XPPAUT code can be downloaded as freeware from www.math.fsu.edu/~bertram/software/neuron. All simulation data available upon request.

Authors' Contributions

KG performed simulations and helped with writing the manuscript. KK performed experiments and helped with writing the manuscript. PQT oversaw the laboratory and helped with writing the manuscript. RB helped with simulations and writing the manuscript.

Ethics Approval

All experiments were carried out in accordance with the National Institutes of Health Guide for the Care and Use of Laboratory Animals (8th edition). Approval was granted by the Florida State University Institutional Animal Care and Use Committee (Date: 12/18/18/Protocol #1845).

1. Introduction

In the brain, information is coded in the spiking patterns of populations of neurons. Input to a neuron from other neurons summates to drive the output of the postsynaptic cell. To a first approximation, this summed input can be thought of as an input current ramp, with the slope of the ramp determined by the degree of synchronicity of firing of the presynaptic neurons. Typically, however, the protocol for analyzing the spiking behavior of a neuron *in vitro* is application of a series of depolarizing current steps (Korshunov et al., 2020; Lübke et al., 1998; Ross et al., 2019). One then quantifies such things as the rheobase (the size of the smallest current step that elicits an action potential), the mean spike frequency, frequency modulation, and amplitude modulation. Neurons can behave as single spikers (no more than one action potential produced during current steps of any magnitude), phasic spikers (transient spiking is followed by a depolarized rest state), or tonic spikers (action potentials continue throughout the current step), among other types. Often, these studies make use of pharmacological agents that block specific types of ion channels or families of ion channels. In some studies, computer simulations are performed to capture these behaviors and provide insight into the contribution that different ion channel types make to the response profile (Carroll et al., 2018; Daou et al., 2013; Golomb et al., 2006).

Although the standard current clamp protocol provides very useful information, the rapid change in applied current followed by a sustained level in the current step are inherently artificial. An alternate approach is to apply rapid depolarizing current ramps, which are closer to physiological input signals; a sniff of duration ~100 ms encodes the information needed to discriminate odors (Cury & Uchida, 2010). We used this approach recently in a study of spiking properties of dopamine (DA) neurons of the olfactory bulb (OB) (Korshunov et al., 2020). Data obtained with this ramp protocol helped to distinguish two types of DA neurons, and provided features of the neurons which were not obtainable from the current step protocol. However, the ramp protocol raises new questions. How can one understand the response of a neuron to a timedependent ramp input? If the peak current is the same but the ramp slope is changed, what differences should be expected in the voltage response? Do the results from slow current ramps (tens of seconds) tell us anything about what is to be expected from much faster, and more physiological, ramps (tens of milliseconds)? As is often the case in neuroscience, the answers to these and related questions are hard to come by, but can be facilitated by the use of a mathematical model neuron. Computer simulations with such a model can replicate behaviors of the actual neurons and, with parameter exploration, can shed light on how the different ion channels affect the response. However, a more systematic, and insightful, approach is to use bifurcation analysis (Sherman, 2011). Such a study summarizes the behavior of the model neuron over a range of parameter values, identifying critical parameter values where there is a qualitative change in behavior. The aim of the present study is to demonstrate how bifurcation analysis can be applied to a model neuron subjected to depolarizing fast or slow current ramps. This analysis explains the spiking pattern produced by the current ramp, and why spiking starts and stops at specific values of the applied current during ramps of varying slopes. That is, it explains why the neuron does what it does during the ramp.

The challenge to analyzing the effects of current ramps, even in mathematical models where all elements of the system are known, is the multi-timescale nature of the gating variables. When slow ramps are applied, all the gating variables are in a quasi-equilibrium state, so the system dynamics can be studied by creating a bifurcation diagram with the applied current (I_{app}) as the bifurcation parameter. This provides summary information on the asymptotic spiking dynamics of the neuron. However, with fast ramps of applied current, some gating variables remain far from

equilibrium throughout the duration of the ramp. This is in contrast to the faster gating variables, such as the Na⁺ channel activation/inactivation variables and the activation variable for the delayed rectifying K⁺ channel, which adjust to the changing applied current much more rapidly and are therefore at quasi-asymptotic states. Because of the presence of the slow gating variables, the neural dynamics may be quite different from the asymptotic dynamics, and a standard bifurcation analysis is therefore potentially misleading.

We demonstrate how a decomposition of the system into fast and slow subsystems, and separate analyses of each, can be used to analyze the response to fast current ramps. Although the model we employ is generic in nature, and not meant to be an accurate representation of any particular neuron, we provide data showing that it captures behaviors seen in actual DA neurons. We also demonstrate the very different properties exhibited by these DA neurons in response to fast vs. slow ramps and how these different behaviors can be understood in terms of the underlying system dynamics through an analysis of the generic model. The approach used here can be employed in higher-dimensional models, including those with several slow gating variables, though the analysis becomes more difficult. Such higher-dimensional fast-slow analyses have recently been performed in other applications (Desroches et al., 2012; Harvey et al., 2011), including other models of excitable cells (Desroches et al., 2012; Hasan et al., 2018; Kimrey et al., 2020b; Rubin & Wechselberger, 2007; Vo et al., 2013).

2. Methods

2.1 Animals

Transgenic hTH-GFP Sprague Dawley rats (Iacovitti et al., 2014)— ages spanning postnatal days 10 to 21 — were used for all experiments (Taconic Biosciences, United States). All neurons expressing the enzyme tyrosine hydroxylase (TH) also express green fluorescent protein (GFP), and are targeted for electrical recordings. In particular, DA neurons of the OB are used in this study. Rats were housed in a controlled, 12-hour light and dark cycle environment, where they received *ad libitum* access to food and water. All experiments were carried out in accordance with the National Institutes of Health Guide for the Care and Use of Laboratory Animals (8th edition), and were approved by the Florida State University Institutional Animal Care and Use Committee.

2.2 Olfactory bulb (OB) dissection

Horizontal OB slices were dissected from rats and used for subsequent electrophysiology recordings from DA neurons. Rats were first anesthetized via isoflurane (Henry Schein Animal Health, Dublin, OH, United States), then promptly decapitated. Their brains were dissected in ice-cold, oxygenated (95% O₂/5% CO₂) sucrose artificial cerebrospinal fluid (sucrose ACSF). The makeup of the sucrose ACSF is as follows (in mM): 83 NaCl, 2.5 KCl, 26.2 NaHCO₂, 1 NaH₂PO₄, 0.5 CaCl₂, 3.3 MgCl₂, 22 glucose, and 72 sucrose. Once extracted, we used a Vibratome (St. Louis, MO, United States) to section 300 μm horizontal OB slices in ice-cold, oxygenated sucrose ACSF. Slices were then incubated in 35°C, oxygenated ACSF for at least 30 minutes. The makeup of ACSF is as follows (in mM): 125 NaCl, 2.5 KCl, 25 NaHCO₂, 1.25 NaH₂PO₄, 2 CaCl₂, 1 MgCl₂, and 25 glucose. The slices were then stored in room temperature until use. Slices were transferred to a recording chamber for all electrophysiology recordings.

2.3 Electrophysiology

A total of 25 rats were used for these experiments (two rats used per electrophysiology recording experiment). Neurons were recorded via whole-cell electrophysiology, exclusively in

current-clamp mode. Recordings were acquired and analyzed with the Multiclamp 700B amplifier (Molecular Devices, Axon Instrument, San Jose, CA, United States), ITC-18 digitizer (Instrutech, Longmount, CO, United States), and the AxographX software (John Clements). OB slices and neurons were visualized via the Leica DMLFS fluorescent microscope (Leica Microsystems, Wetzlar, Germany) and the Hitachi HV-D30 camera (B&H, NY, United States).

Recording electrodes were pulled from borosilicate glass (World Precision Instruments, Sarasota, FL, United States), with a final tip resistance of 4-6 M Ω . The makeup of the intracellular recording solution is as follows (in mM): 125 KMeSO₄, 0.025 CaCl₂, 2 MgCl₂, 1 EGTA, 2 Na₂ATP, 0.5 NaGTP, and 10 HEPES. OB slices were constantly perfused with oxygenated ACSF at the rate of ~1 ml/minute. A total of 26 OB neurons were used for this study.

We used a combination of step and ramp current-clamp protocols of different durations and amplitudes to analyze the transient and asymptotic properties of the DA neurons. The step protocols used included incremental injections of 10 pA (from -10 to 80 pA), 25 pA (from -25 to 200 pA), or 50 pA (from -50 to 400 pA) steps, which had the durations of either 300 or 500 ms. In ramp protocols, current stimuli gradually increased to their maximum value for a specified amount of time. For these experiments on transient activity, we used ramps of 0.167, 0.25, 6, and 12 pA/ms (100 pA over 600 ms, 100 pA over 400 ms, 300 pA over 50 ms or 600 pA over 100 ms, and 600 pA over 50 ms, respectively) slopes to record the transient activity of neurons. To record the asymptotic activity of neurons, ramps with much smaller slopes and longer durations were used. For these experiments, we used ramps with slopes of 0.00125, 0.0025, and 0.0033 pA/ms (75 pA over 60 seconds, 150 pA over 60 seconds, and 100 pA over 30 seconds, respectively).

2.4 The mathematical model

We employed a simple Hodgkin-Huxley-based single-compartment neuron model, modified from (Dovzhenok & Kuznetsov, 2012). There are four voltage-gated ionic currents: a delayed-rectifying K⁺ current (I_K), a Na⁺ current (I_{Na}), a slowly-activating K⁺ current (I_{KS}), and a leak current (I_L). The currents are determined largely by four gating variables: a fast K⁺ channel activation variable (n), a slow K⁺ channel activation variable (z), a Na⁺ channel activation variable (m), and a Na⁺ channel inactivation variable (n). Since Na⁺ channel activation is much faster than other gating processes, we employ the quasi-equilibrium approximation in which m is replaced by its steady state function, $m_{\infty}(V)$. Since the Na⁺ channel inactivation variable is approximately linearly related to the fast K⁺ channel activation variable, we replace n0 with this linear function of n1. The equations for ionic currents are then

$$I_K = g_K n^4 (V - V_K) \tag{1}$$

$$I_{Na} = g_{Na} m_{\infty}^3 h (V - V_{Na}) \tag{2}$$

$$I_{KS} = g_{KS}z(V - V_K) \tag{3}$$

$$I_L = g_L(V - V_L) \tag{4}$$

$$h = 0.1 - 0.5(n - 0.8). (5)$$

There are nonlinear differential equations for the three variables V, n, and z, as shown below. The applied current, I_{app} , is either a depolarizing step function (9) or a linearly increasing ramp current (10).

$$\frac{dV}{dt} = -\frac{1}{C} \left(I_K + I_{Na} + I_{KS} + I_L - I_{app} \right)$$
 (6)

$$\frac{dn}{dt} = \frac{n_{\infty} - n}{\tau_n} \tag{7}$$

$$\frac{dz}{dt} = \frac{z_{\infty} - z}{\tau_z} \tag{8}$$

$$I_{app} = X \tag{9}$$

$$I_{app} = \text{slope-T}$$
 (10)

where X > 0 in equation (9) is the size of the current step (in pA) and T in equation (10) is the time since the initiation of the ramp (in ms). The equilibrium functions for the gating variables, and the V-dependent time constant τ_n are:

$$m_{\infty} = \frac{1}{\frac{-(V - v_{mh})}{1 + e^{-S_m}}} \tag{11}$$

$$n_{\infty} = \frac{1}{1 + e^{\frac{-(V - v_{nh})}{s_n}}} \tag{12}$$

$$z_{\infty} = \frac{1}{1 + e^{\frac{-(V - v_z)}{S_z}}}$$
 (13)

$$\tau_n = \tau_{n_0} + \tau_{n_1} e^{\frac{-(V - \theta_n)^2}{S_{n\tau}}}$$
 (14)

The activation variable z changes much more slowly than the variables V and n due to its large time constant (50 ms versus < 6 ms for the other activation variable, n). Because of this, during a burst of spikes the z variable slowly accumulates, and slowly falls afterwards (shown later).

Model parameters are listed in Table 1, and the differential equations were solved numerically using XPPAUT (available at www.math.pit.edu/~bard/xpp/xpp.html) using the Dormand-Prince solver. The XPPAUT code can be downloaded as freeware from www.math.fsu.edu/~bertram/software/neuron.

Table 1: Model Parameters		
Parameter	Value	
С	1 pF	
$ au_z$	50 ms	
g_{κ}	40 nS	
g_{Na}	120 nS	
g_L	0.3 nS	

g _{KS}	110 nS (single spiker)	5 nS (tonic spiker)
V_K	-77 mV	
V_{Na}	55 mV	
V_L	-44.4 mV	
v_{mh}	-40 mV	
v_{nh}	−53 mV	
v_z	−45 mV	
S_m	9 mV	
S_n	15 mV	
S_Z	10 mV	
$s_{n au}$	50 mV^2	
$ au_{n_0}$	1.1 ms	
$ au_{n_1}$	4.7 ms	
θ_n	−53 mV	

3. Results

3.1 The slowly-activating K^+ conductance can determine whether a neuron is a single spiker or a tonic spiker

The experimental voltage traces shown in Fig. 1 illustrate the two characteristic behaviors observed in *in vitro* recordings of DA neurons in response to a step of depolarizing current: the cell may respond with a single action potential or spike (referred to as single spikers, Fig. 1A,B) or with a train of spikes (referred to as tonic spikers, Fig. 1C,D). With small depolarizing current steps, neither type of cell reliably produces an action potential. With sufficiently large steps, single spikers typically respond with a single spike, regardless of the size of the step. Tonic spikers typically produce a continuous train of spikes, but may enter depolarization block with sufficiently large input. These are the defining behaviors of the two types of neurons that were characterized previously in the OB DA neurons (Korshunov et al., 2020). Since such current steps are artificial, we examined how the two types of neurons responded to current ramps, in which the applied current was increased linearly from 0 to some ending value. The ramp protocol was then parameterized by the slope of the ramp. The single spiker shown in Fig. 1 responded to a current ramp with a single spike when the ramp slope was large (12 pA/ms, Fig. 2A), and with a small voltage deflection, but not a full-blown spike, when the ramp slope was small (0.25 pA/ms, Fig. 2B). In several other cells of this type, single spikes were produced at both ramp slopes. The difference in the response of the tonic spikers to current ramps of small or large slopes was typically more dramatic, and this is reflected in the example of Fig. 2C, D. When the ramp slope was large, the neuron responded with a spike and two small-amplitude spikes as it approached depolarization block (Fig. 2C). When the slope was small, more spikes were invariably produced, often followed by depolarization block (Fig. 2D). Although only representative examples are shown here, their behaviors are characteristic of the population of OB DA neurons studied, as described in (Korshunov et al., 2020). These behaviors motivated us to understand the effects of current ramps on single spikers and tonic spikers from a mathematical perspective, using a generic neural model for the analysis. Why do single spikers remain single spikers when stimulated with a current ramp? Why do tonic spikers produce fewer spikes when the ramp slope is greater? Why does the cell stop spiking when it does, and is this different depending on the slope of the current ramp? These are the experimental questions we wished to answer. The mathematical focus of the study was to determine an effective way to analyze the dynamics underlying application of ramped input in a model neuron consisting of both fast and slow gating variables. The model we employed has the minimal set of components needed to achieve these goals.

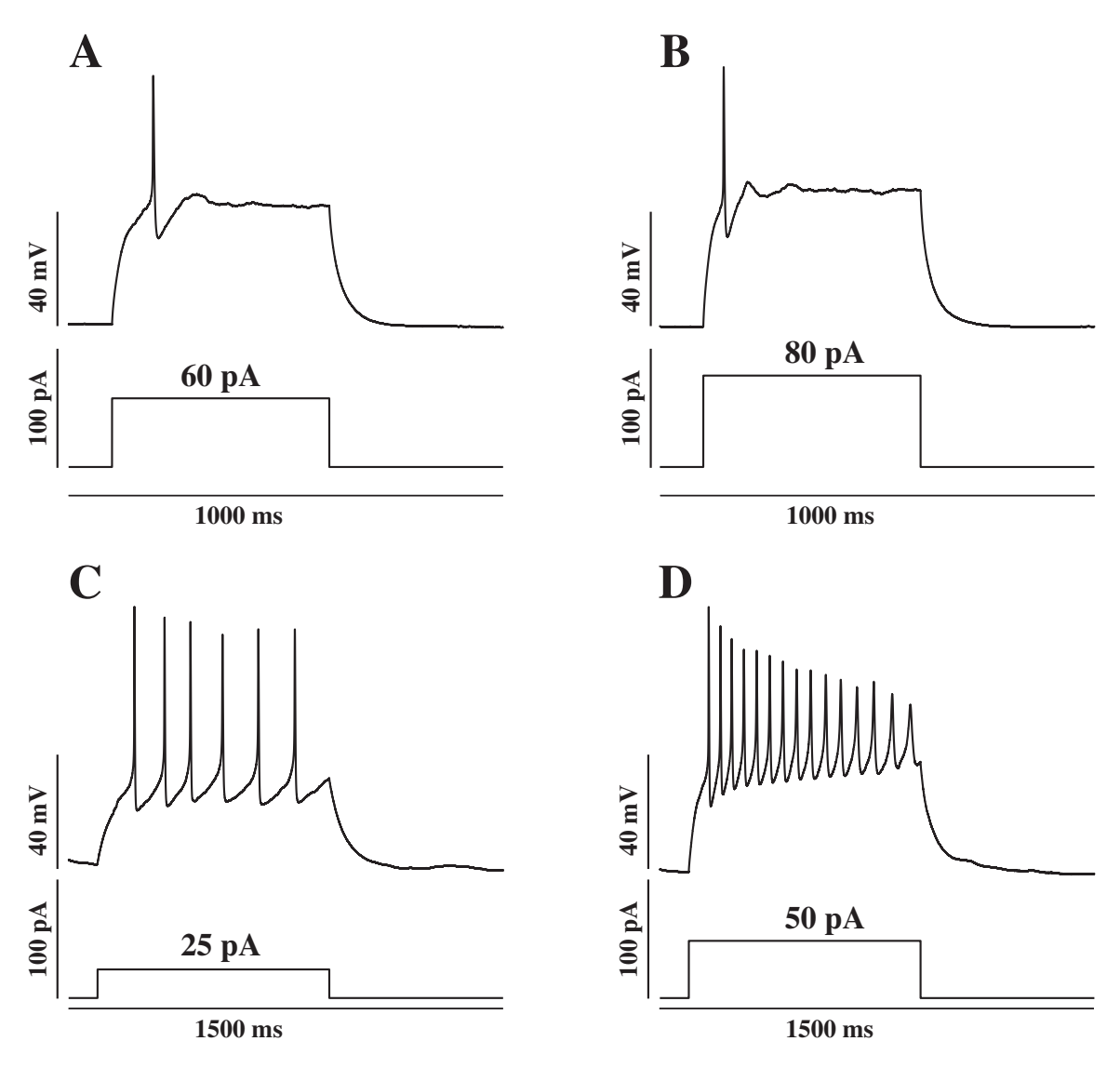


Fig. 1: Patch clamp recordings demonstrating the two characteristic behaviors observed in DA neurons in response to a step of depolarizing current. (A, B) Single spiking response to steps of depolarizing current (60 and 80 pA, respectively). (C, D) Tonic spiking responses to depolarizing current steps (25 and 50 pA, respectively).

To differentiate between the two different types of neurons, we changed a single parameter in the model: the conductance of the slowly-activated K^+ current (g_{KS}) . We found that single spiker behavior was achieved with large values of g_{KS} , while tonic behavior was produced with small values of g_{KS} . This is illustrated in Figure 3. When depolarizing current steps of 150 pA or 250 pA were simulated (Fig. 3A), the model cell responded with a single spike when $g_{KS} = 110$ nS (Fig. 3B). In contrast, when the same input steps were applied to the model neuron with $g_{KS} = 5$ nS, tonic spiking was produced (Fig. 3C). Biophysically, when the conductance of the slowly activated K^+ current is large, the hyperpolarizing K^+ current reaches a sufficiently large value after the first spike to prevent the membrane potential from reaching spike threshold, so a second spike is not produced.

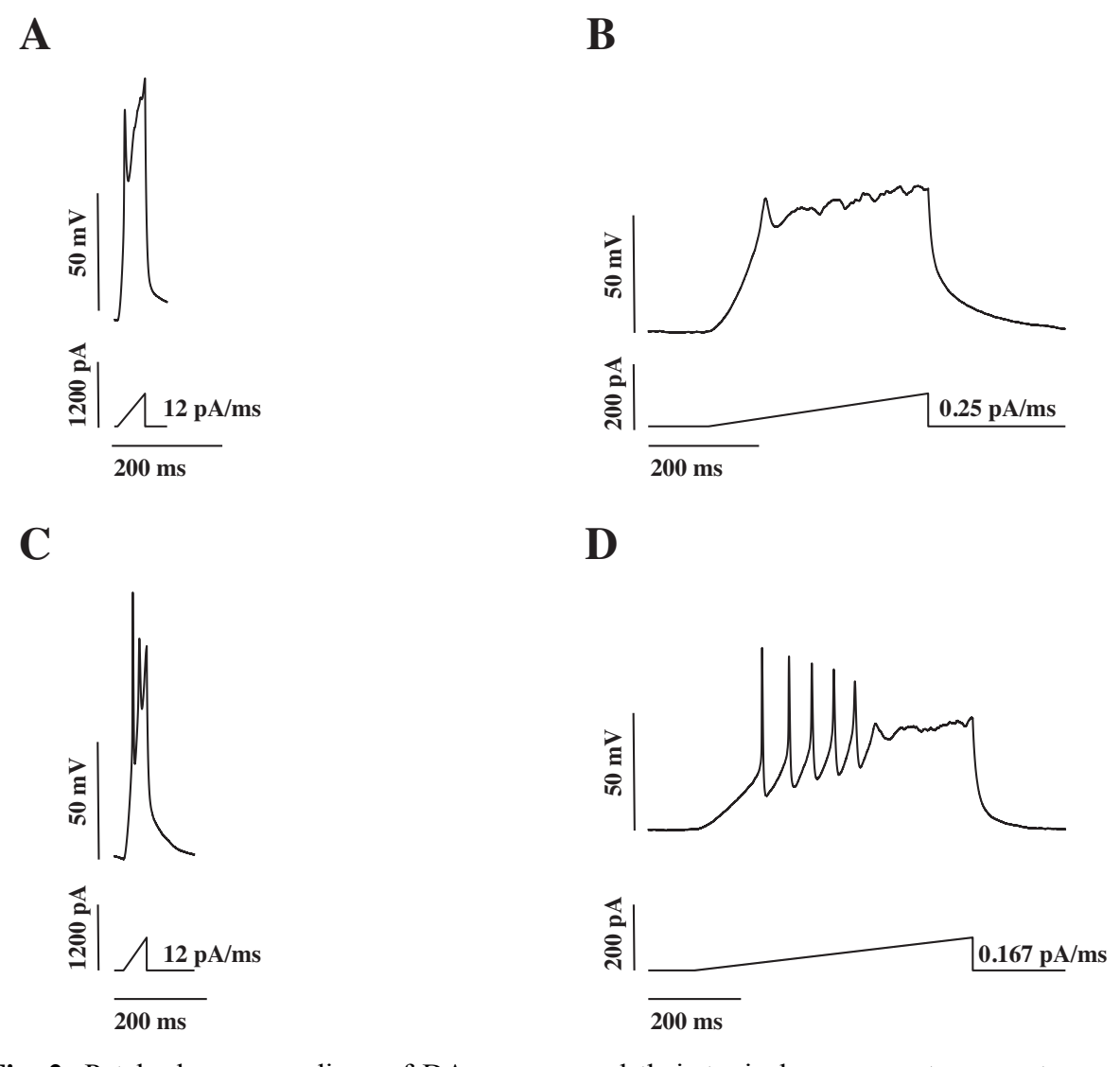


Fig. 2: Patch clamp recordings of DA neurons and their typical responses to current ramps. Neurons that respond to current steps with a single spike, i.e., the single spikers, respond to current ramps with a single spike (A, B). Neurons that respond to current steps with continuous spiking, i.e., the tonic spikers, respond quite differently to current ramps. The number of spikes produced is less during a ramp with large slope (C) than to a ramp with small slope (D).

The model also captures the overall behavior observed in experiments in response to a ramped applied current. For a single spiker (i.e., a model cell with $g_{KS} = 110$ nS), when given a ramp of applied current with a large slope (Fig. 3D, black), a single spike is produced (Fig. 3E, black). When the current ramp has a smaller slope (Fig. 3D, green), the model cell does not spike at all (Fig. 3E, green). Model tonic spiking neurons produce a train of spikes followed by depolarization block when ramps of applied current are simulated with large slopes and small slopes. However, the number of spikes produced during the large-slope ramps is less that the number produced during the small-slope ramps (Fig. 3F). Thus, these model neurons capture the basic spiking behavior for single and tonic spikers.

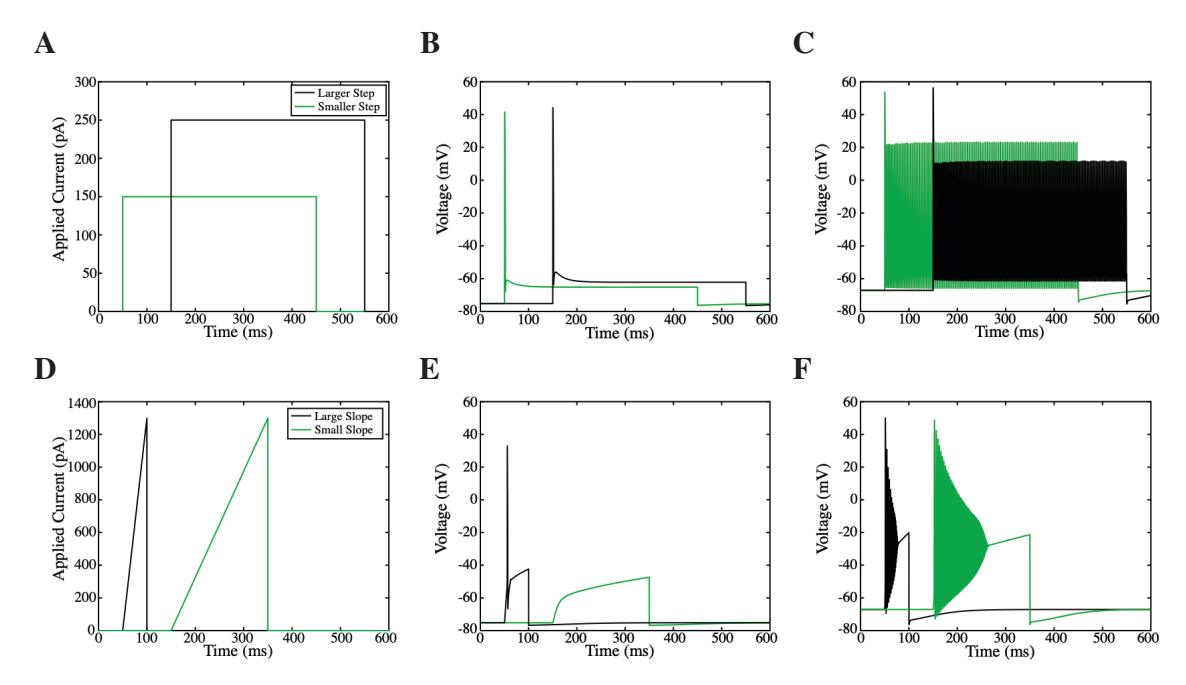


Fig. 3: Simulations of model neurons in response to current steps and ramps. (A) Current steps of two different sizes, offset in time for clarity. (B) Model single spikers ($g_{KS} = 110 \text{ nS}$) produce a single spike in response to each current step. (C) Model tonic spikers ($g_{KS} = 5 \text{ nS}$) respond to current pulses with a train of action potentials. (D) Current ramps with slope of 26 pA/ms (black) and 6.5 pA/ms (green). Values of the maximum applied current and ramp duration where chosen arbitrarily, but the maximum current value is the same for both ramps. (E) A single spiker responds to the ramps with either a single spike or no spike at all. (F) A tonic spiking neuron produces fewer spikes during a large-slope ramp than during a small-slope ramp, as seen in experiments (Fig. 2).

3.2 Bifurcation analysis shows agreement between the asymptotic dynamics of the model and the experimental data

Before examining the basis of the transient response to current ramps, we investigated the simpler case of the asymptotic, or long-term, spiking properties of the neurons. The asymptotic dynamics of the model neuron can be illustrated through the use of a bifurcation diagram, treating the applied current, I_{app} , as a bifurcation parameter. The bifurcation diagram for the model single spiker is shown in Fig. 4A. In this case, there is a stable equilibrium for all values of I_{app} (red

curve), indicating lack of a tonic spiking interval so that any spikes produced during short steps or ramps reflect transient properties of the cells. In contrast, for the model tonic spiker, there is an interval of applied current values where the equilibrium is unstable and there is a branch of stable periodic solutions (Fig. 4B). This interval is delimited by a subcritical Hopf bifurcation on the left and a supercritical Hopf bifurcation on the right. For each value of I_{app} between the Hopf bifurcations, the model neuron responds with tonic spiking (green curves indicate minimum and maximum values of V during oscillations).

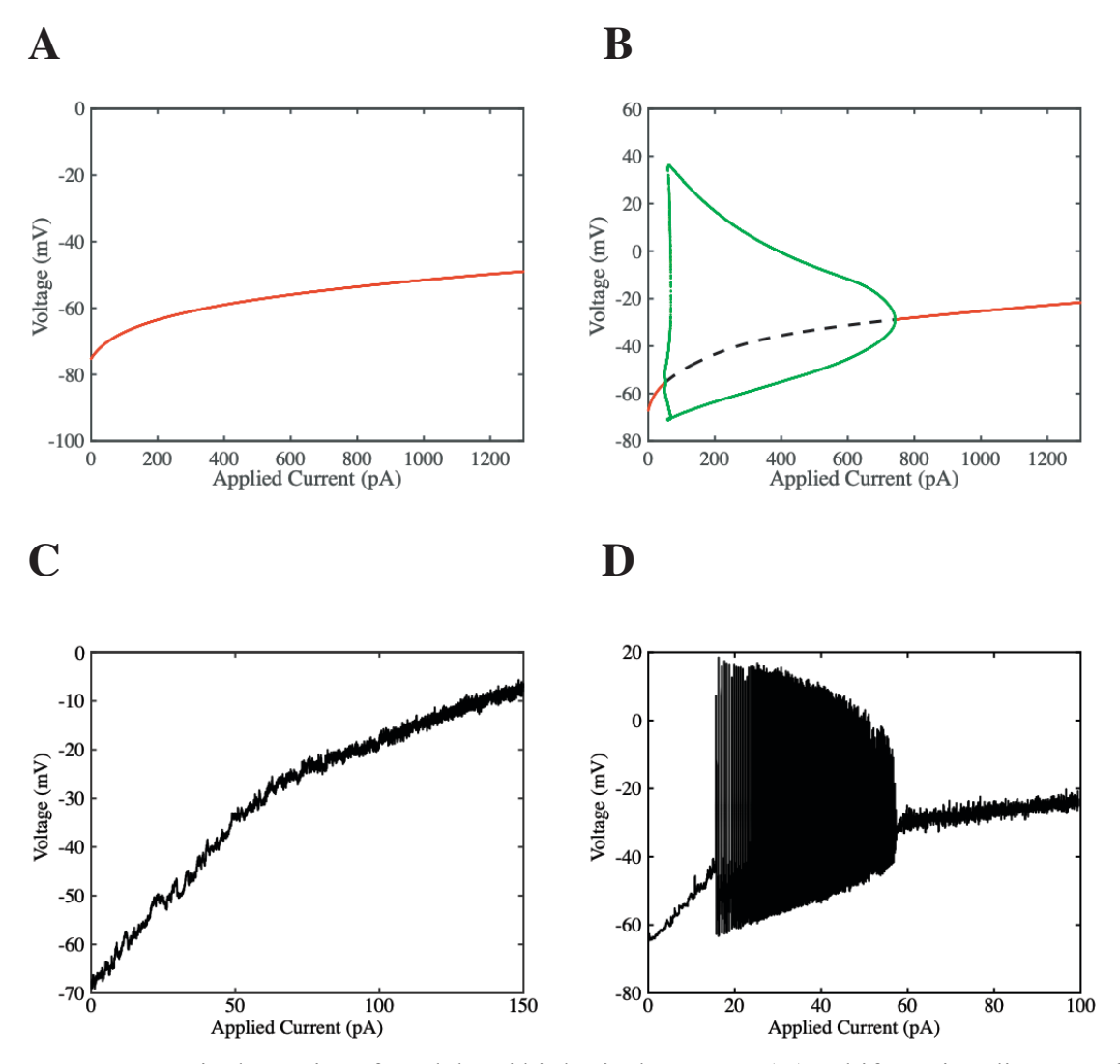


Fig. 4: Asymptotic dynamics of model and biological neurons. (A) A bifurcation diagram of the model single spiker indicates that there is a single stable equilibrium at all current values. The neuron becomes more depolarized with greater applied current, but there are no current values that elicit tonic spiking. (B) In the model tonic spiker, there is a large range of current values for which a stable periodic, or tonic spiking, behavior is produced. (C) An experimental bifurcation diagram produced using a slow ramp of depolarizing current. A single spiker exhibits a stable resting voltage for the full range of applied current. (D) The experimental bifurcation diagram for a tonic spiking neuron exhibits a range of applied current for which tonic spiking occurs.

Do DA neurons exhibit similar asymptotic dynamics *in vitro*? To check, we applied slowly ramped current at a rate of 0.0025 pA/ms over a duration of 60 seconds (Fig. 4C), and at a rate of 0.00333 pA/ms over the duration of 30 seconds (Fig. 4D). These ramps are much slower than the ramps of Fig. 2. For a single spiker, the experimental bifurcation diagram shows a curve of resting states, becoming more depolarized as the applied current is increased (Fig. 4C). As with the model bifurcation diagram for the single spiker, there is no spiking interval. In contrast, for a tonic spiker, the bifurcation diagram exhibits a large spiking interval between roughly $I_{app} = 20$ pA and 60 pA (Fig. 4D). For any of these applied current values, the neuron produces tonic spiking.

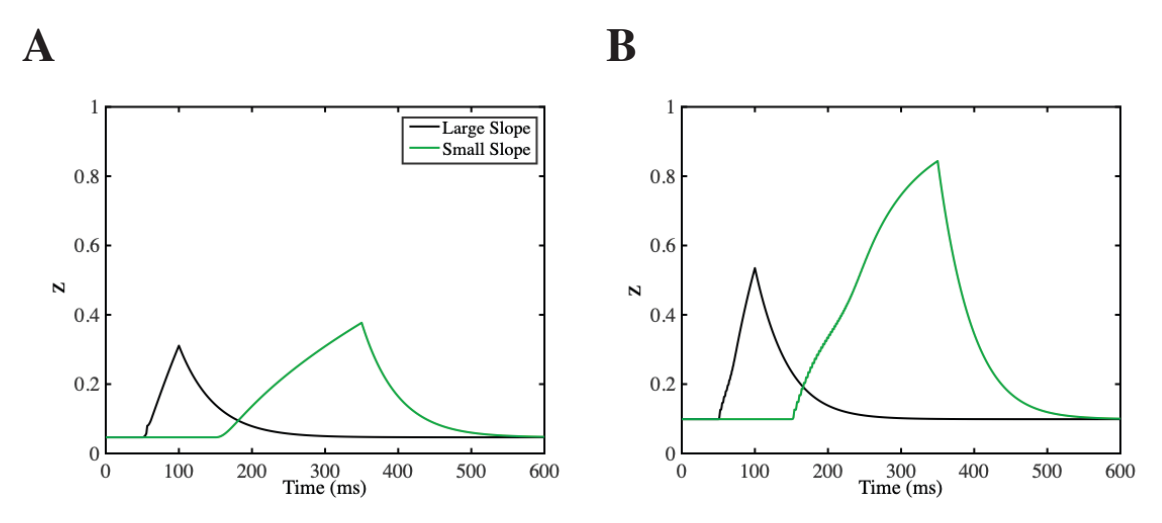


Fig. 5: The response of the activation variable for the slowly activated K^+ channels (z) during large-slope (black, 50 ms duration) and small-slope (green, 200 ms duration) current ramps. (A) In the model single spiker, z increases slowly during the current ramps. (B) There is a similar slow increase in z in the model tonic spiker, but there is now a change in slope when the model neuron enters depolarization block.

3.3 Towards an understanding of transient dynamics using bifurcation analysis of the fast subsystem

The bifurcation analysis performed in Fig. 4 is informative, since it tells in a succinct manner the values of the input current at which stationary or tonic spiking behavior occurs in the model or biological neuron. Unfortunately, it says little to nothing about what to expect during fast current ramps. For example, the single spiker bifurcation diagrams predict no spiking, yet in both the model and biological cells, single spikes often occurred during fast ramps. The experimental bifurcation diagram for the tonic spiker predicts that tonic spiking should occur for I_{app} up to ~57 pA. The spiking that occurs for the ramp with the small slope in Fig. 2D terminates at a similar value (~70 pA), but these are significantly different from the termination point with the large slope ramp in Fig. 2C (~473 pA). The experimental bifurcation diagram for the tonic spiker predicts that tonic spiking should occur for I_{app} up to ~57 pA, but in the fast ramps the spiking stopped at significantly lower values (~473 pA for the ramp with large slope, Fig. 2C, and ~70 pA for the ramp with small slope, Fig. 2D). Similarly, in the model, the spiking branch of the bifurcation diagram terminates at an I_{app} value (the right Hopf bifurcation is at 743 pA in Fig. 4B) that is different from that of the tonic spikers with the fast ramps. Indeed, the value of I_{app} at which spiking stops is different in the fast ramp with large slope (736 pA) than that in the fast ramp with

small slope 761 pA, Fig. 3F), and this cannot be explained by the asymptotic bifurcation diagram of Fig. 4B.

Although bifurcation analysis of the asymptotic dynamics clearly fails to describe the transient dynamics that occur during fast current ramps, might it be possible to adapt bifurcation analysis to capture transient dynamics in the model where the time courses of all variables are known? The challenge to doing this is that variables that change on slow time scales don't reach equilibrium over the timescale of the fast ramp, so if one assumes that an equilibrium is reached (as in the asymptotic bifurcation analysis) the results will be misleading, as we have seen. To account for the dynamics of the slow variables, it is therefore necessary to determine a functional relationship between the value of each slow variable and the applied current. In our model, there is only one variable that changes on such a slow time scale for this to be a concern, the activation variable for the slowly activated K^+ channels (z). In what follows, we derive such a relation. Once done, bifurcation analysis of the fast subsystem of variables (V and v) can be performed, using V0 as a bifurcation parameter with v1 slaved to V1 and v2 slaved to V3 and v3 are between the derived relation.

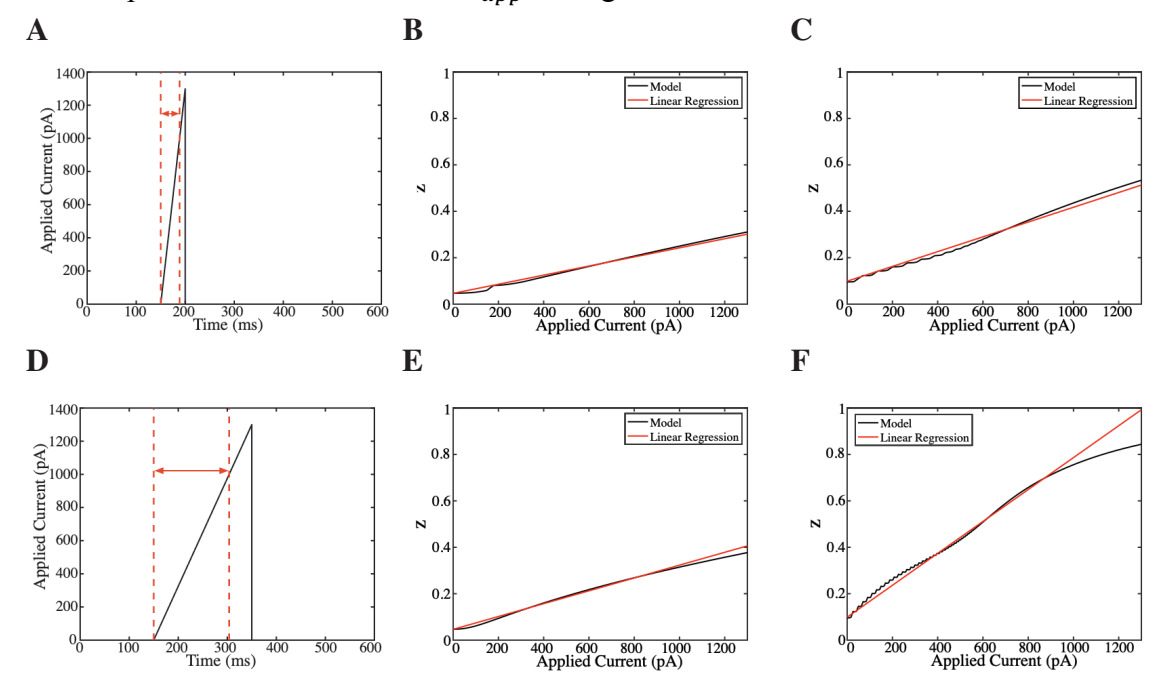


Fig. 6: Linear regression analysis was used to establish the linear dependence of z on the applied current. This relationship was fit over the duration of the ramp up to $I_{app} = 1000$ pA. (A, D) Range of fit over large-slope and small-slope current ramps, respectively, is indicated by the red dashed lines. (B, E) The activation variable (black) for a model single spiker had an almost-linear dependence on applied current during the large-slope and small-slope ramps, respectively. (C, F) The z activation variable for the model tonic spikers also exhibited an almost-linear dependence on applied current during large-slope and small-slope ramps, respectively. For each linear regression estimation, β_0 from equation (15) was fixed to be the initial z value prior to the start of the ramp and the estimation of the time course by the linear regression estimate has an $R^2 > 0.95$.

The response of z to ramps of applied current is shown in Fig. 5, for both the single spiker (Fig. 5A) and the tonic spiker (Fig. 5B). The variable increases due to the rise in V induced by the current ramp, but in neither case is there evidence of action potentials, since z changes slowly and the effects of fast fluctuations in voltage are averaged out. In the case of the tonic spiker, there is a noticeable change in the positive slope in z when the model cell stops spiking and enters depolarization block.

The time course of z during the fast ramps looks approximately linear, which motivated us to apply a linear regression on each of the traces (Fig. 6) and thereby establish an approximate affine relationship between z and I_{app} . In the regression equation,

$$z = \beta_1 I_{app} + \beta_0 \tag{15}$$

 β_0 was fixed to be the initial z value prior to the start of the ramp. The slope of the linear approximation, β_1 , was estimated using a subset of values of the I_{app} ramp ($I_{app} \in [0, 1000]$ pA) and produced a linear fit with an $R^2 > 0.95$. Values of β_1 for both types of neurons and for both ramp slopes are provided in Table 2.

Table 2: Linear Regression Slope (β_1) for Ramp Duration			
Total Ramp Duration	Single Spiker β ₁ Value	Tonic Spiker β_1 Value	
25 ms	1.335×10^{-4}	1.877×10^{-4}	
50 ms	1.96×10^{-4}	3.185×10^{-4}	
75 ms	2.226×10^{-4}	4.196×10^{-4}	
100 ms	2.405×10^{-4}	4.989×10^{-4}	
125 ms	2.535×10^{-4}	5.619×10^{-4}	
150 ms	2.632×10^{-4}	6.125×10^{-4}	
175 ms	2.707×10^{-4}	6.537×10^{-4}	
200 ms	2.766×10^{-4}	6.876×10^{-4}	
225 ms	2.814×10^{-4}	7.157×10^{-4}	
250 ms	2.854×10^{-4}	7.393×10^{-4}	
275 ms	2.887×10^{-4}	7.593×10^{-4}	

The fit to the z time course of the single spiker is shown in Fig. 6B for a large-slope ramp and Fig. 6E for a small-slope ramp (time course in black, regression line in red) and the fit to the tonic spiker is shown in Fig. 6C during a large-slope ramp and in Fig. 6F during a small-slope ramp. All fits appear to be quite good, at least over the range of I_{app} values examined (up to 1000 pA). Since the values of I_{app} where spiking starts and stops are less than 1000 pA, and these are the most important features, the regression fits should be satisfactory.

An increase in the duration (decrease in slope) of the applied current ramp resulted in a larger value of β_1 for both single spiking and tonic spiking neurons (Table 2). This relationship is plotted in Fig. 7 for both types of neurons. Also shown in the figure are Michaelis-Menten fits to the points, using (16) where D is duration, A is the maximum value of β_1 , k is the duration when the half maximum value of β_1 is achieved, and both A and k are estimated with an $R^2 > 0.95$, as reported in the figure caption. Now, using this newly determined relationship, z can be expressed

in terms of its initial value prior to the current ramp, the duration of the current ramp, and I_{app} as it changes during the ramp. With this relationship, the differential equation for z (8) can be removed and replaced by

$$z = \left(\frac{A \cdot D}{k + D}\right) I_{app} + \beta_0 \quad . \tag{16}$$

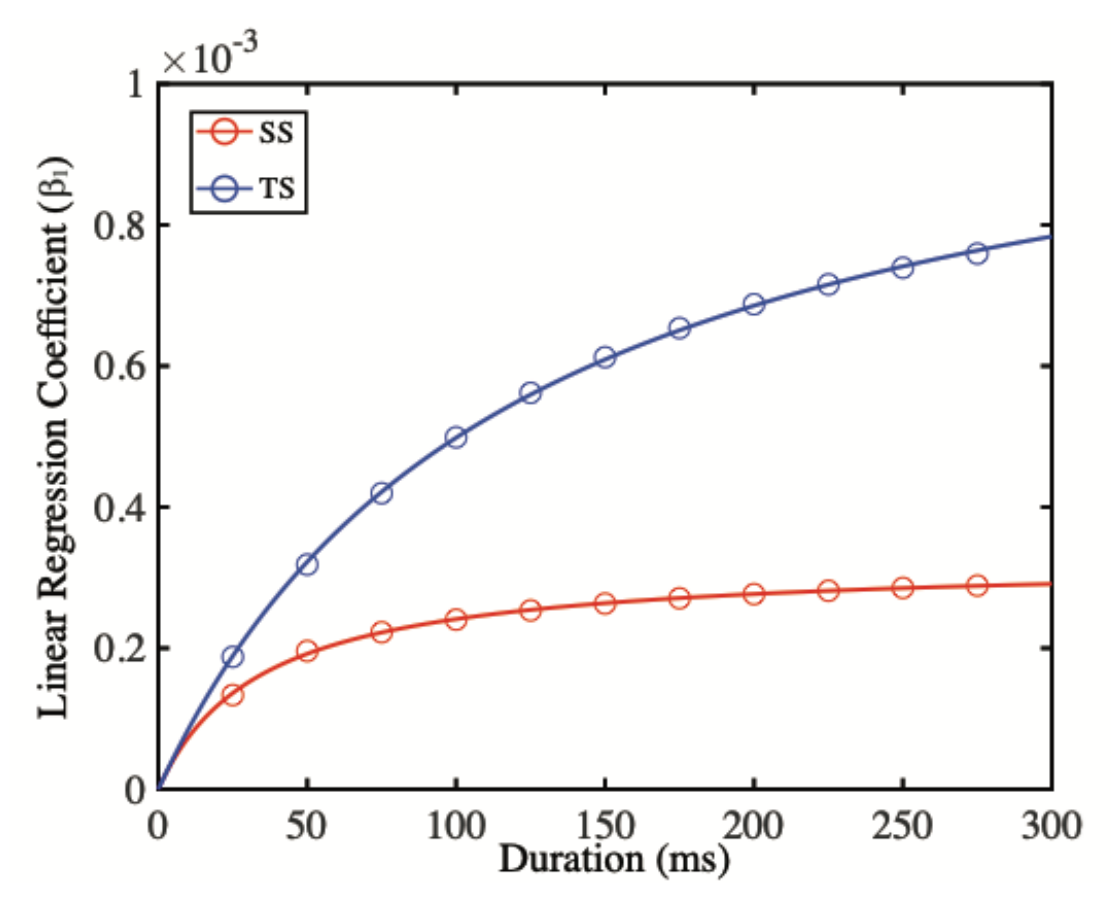


Fig. 7: Increasing the duration of the applied current ramp resulted in a larger value of β_1 for both types of neurons. The value of β_1 corresponding to each ramp duration is shown by an open circle for both single spikers (SS) and tonic spikers (TS). This was fit with a Michaelis-Menten function (solid line through points). The parameter values for this fit are: $A = 3.2448 \times 10^{-4}$ (single spiker), 1.098×10^{-3} (tonic spiker), and k = 34.5019 (single spiker), 120.3198 (tonic spiker).

3.4 Using fast-subsystem bifurcation analysis to understand spiking behavior in response to fast ramps of applied current

With the functional relationship between z and I_{app} described through (16) for fast ramps with arbitrary slopes (with durations up to 300 ms), it is now possible to analyze the dynamics of the model neuron using bifurcation analysis of the system (6), (7), and (16). In particular, we can now use bifurcation analysis to understand why each type of neuron responds the way that it does to ramps with different slopes. Figure 8 shows how the membrane voltage of a model single spiker changes in response to the applied current if given a large-slope ramp (50 ms duration, Fig. 8A),

or a ramp with small slope (200 ms duration, Fig. 8B). In both cases, there is a branch of stable stationary solutions with no periodic branch, indicating a lack of tonic spiking at any point along the current ramp. The single spike that occurs for some large ramp slopes (e.g., Fig. 3E) is not captured by the bifurcation diagram since it is not an asymptotic behavior of the fast V-n subsystem, which is what the bifurcation diagram of Fig. 8 reflects. That is, it is a product of a very fast change in V during a spike upstroke and a slower change in n that is responsible for the downstroke. In the bifurcation diagram, both V and n are at equilibrium states. As a comparison with the bifurcation diagram of the full 3-dimensional system during a slow ramp of applied current we superimpose the bifurcation diagram from Fig. 4A as dashed curves. Notice that the curve for the slow ramp is below that of the fast ramp, since in this case the z variable is at an equilibrium value that is larger than its value during the fast ramp. Since this is the activation variable for a hyperpolarizing current, it brings the voltage to a lower value.

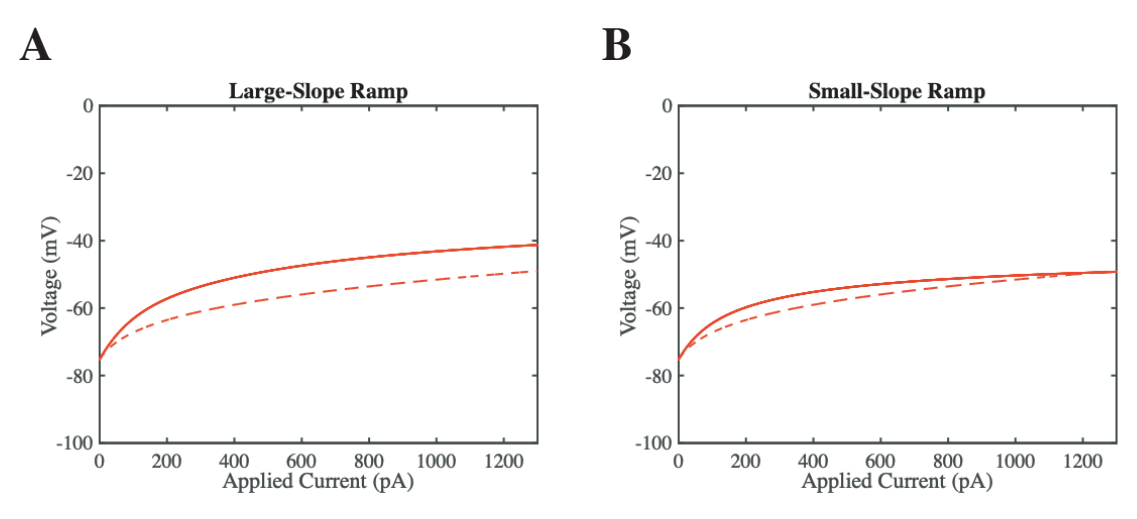


Fig. 8: Bifurcation analyses of the model single spiker neuron ($g_{KS} = 110 \text{ nS}$) to fast ramps of applied current are shown with a solid red curve in (A) and (B). Equations (6), (7), and (16) were used. Dashed curves are from the bifurcation analysis of Fig. 4A, corresponding to a slow ramp of I_{app} . (A) Response to a large-slope (50 ms duration) ramp shows no spiking interval. (B) Response to a small-slope (200 ms duration) ramp is similar.

The bifurcation diagram for the model tonic spiker is more interesting. For both a large-slope ramp (Fig. 9A) and a small-slope ramp (Fig. 9B), there is a branch of periodic solutions, reflecting tonic spiking. The periodic branch is born at a subcritical Hopf bifurcation and terminates at a supercritical Hopf bifurcation. The value of I_{app} at which the supercritical Hopf bifurcation occurs ($I_{app} = 666 \, \text{pA}$) is approximately the same for both ramps. Therefore, differences in the size of the spiking interval does not explain why large-slope current ramps elicit fewer spikes than do the small-slope ramps. Neither is it explained by differences in frequency response over the range of applied currents, which is similar for the two ramps (Fig. 9C, D). In both cases, the spike frequency increases with increasing I_{app} , peaking at ~1.2 mHz for both ramps. Instead, the difference in spiking behavior between large-slope and small-slope ramps comes from the amount of time spent within the spiking interval. For a large-slope ramp, I_{app} changes rapidly, so the system is swept through the spiking interval quickly, eliciting only a few spikes. This is illustrated by the long arrows in Fig. 9A. For the small-slope ramp, I_{app} changes more slowly, so progression through

the spiking interval takes longer, eliciting more spikes (illustrated with short arrows in Fig. 9B). Thus, the fast-slow analysis explains one of the key findings of both the model and the biological neuron.

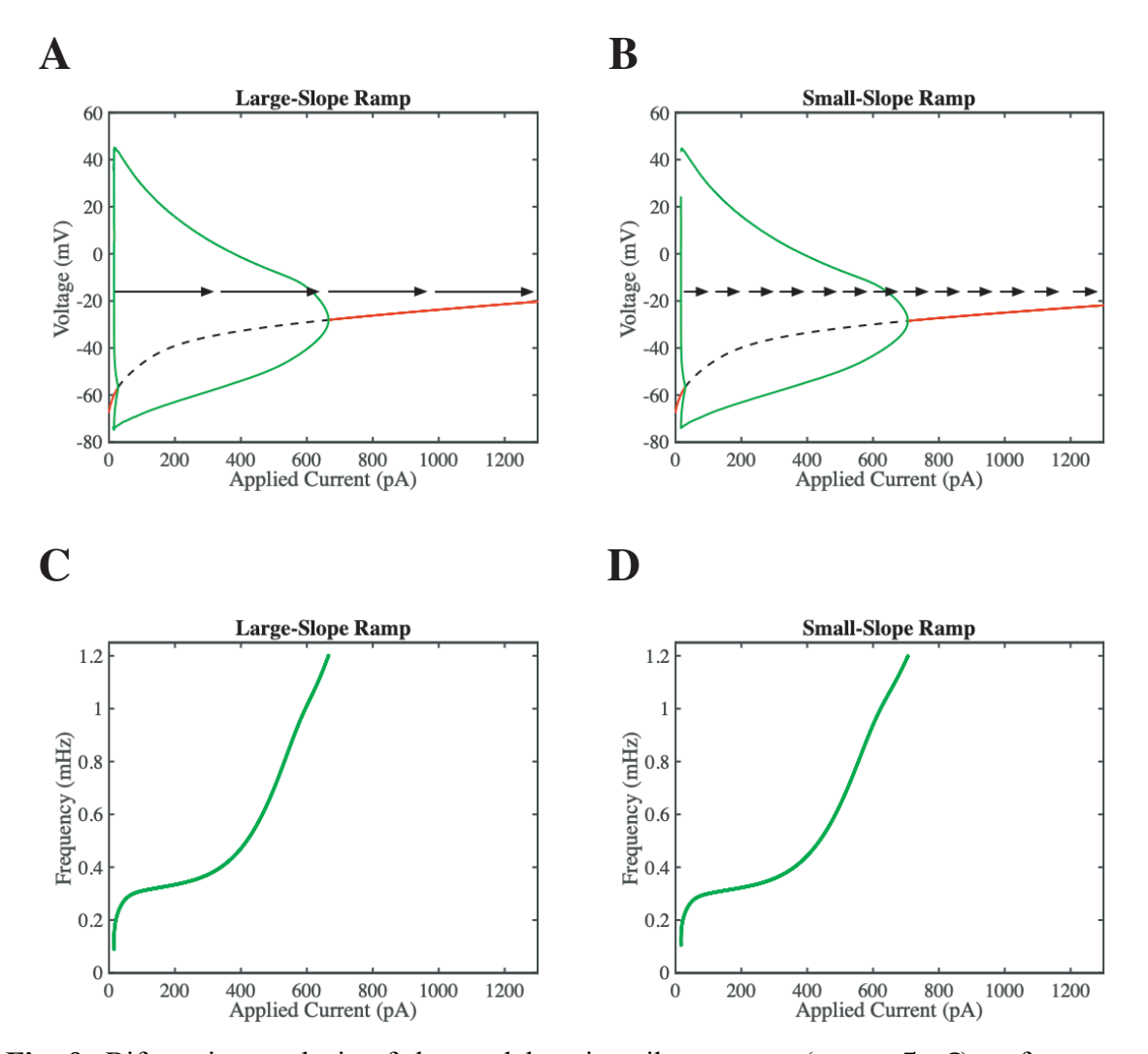


Fig. 9: Bifurcation analysis of the model tonic spiker neuron ($g_{KS} = 5 nS$) to fast ramps of applied current. Equations (6), (7), and (16) were used. (A) Response to a large-slope (50 ms duration) ramp shows a branch of stable periodic spiking solutions, delimited on the left by a subcritical Hopf bifurcation and on the right by a supercritical Hopf bifurcation. The applied current changes rapidly during the ramp, illustrated by the long arrows. (B) Response to a small-slope (300 ms duration) ramp is very similar, but now the change in applied current during the ramp is much slower. Illustrated with small arrows, whose length is scaled to reflect the speed of the phase point. The asymptotic spike frequency over the range of the periodic branch is shown in (C) and (D). As the applied current is increased, the frequency of spiking increases for both ramps, peaking at ~1.2 mHz for both a large-slope ramp and a small-slope ramp.

Because both the ramp duration and the applied current appear in the equation (16) for the slow variable z, it is possible to determine how the tonic spiking interval varies with the duration of the ramp (or its inverse, the ramp slope). This is done through the construction of a two-parameter

bifurcation diagram, in which the two Hopf bifurcations initiating and terminating the periodic tonic spiking branch are continued in ramp duration D (Fig. 10A). The leftmost blue curve in Fig. 10A is nearly vertical, which indicates that the subcritical Hopf bifurcation that initiates the spiking interval is almost independent of the ramp duration (or slope). This is an intuitive result, since the spiking starts shortly after the beginning of a current ramp, regardless of the ramp slope. The termination point does vary with ramp duration, taking on larger values at longer durations (and smaller ramp slopes). This indicates that the neuron goes to a state of depolarization block at larger applied current values when the current ramp is slower. This is true because at slower ramp speeds the z activation variable achieves larger values at each value of the applied current (closer to its equilibrium level), and the resulting hyperpolarizing current works to prevent depolarization block. Overall, the region of tonic spiking for this type of neuron is large, ensuring that ramps of a wide range of slopes will elicit spikes in these model neurons. The ramp durations used in previous figures are shown as dashed horizontal lines; the bottom line was referred to as a "large-slope ramp", while the top line was referred to as a "small-slope ramp".

Although the analysis of Fig. 8 for single spikers did not show a spiking interval, such an interval does exist for shorter ramp durations. As shown in Fig. 10A (red curve), there is a small region of the two-parameter plane in which spiking would occur in single spikers. In contrast, for the tonic spiker the Hopf bifurcations never coalesce; as the ramp slope is made arbitrarily small the fast-subsystem bifurcation diagram approaches the asymptotic one (Fig. 4B), which has two Hopf bifurcations.

3.5 A hypothetical third type of neural response to fast current ramps

We have seen in both model and biological neurons two response types to fast current ramps. In one type, either a single spike or no spike is produced. In the other type, the number of spikes elicited is smaller during a large-slope ramp than during a small-slope ramp. Our analysis shows, however, that a third type of response is possible. Here, the number of spikes produced is *larger* during a large-slope ramp than during a small-slope ramp. Although we found no instances of this response in our electrophysiological recordings, it is at least theoretically possible if the twoparameter bifurcation structure is similar to the black curve in Fig. 10B, which was generated using an intermediate value of the slowly activated K^+ conductance ($g_{KS} = 50$ nS). "intermediate neuron," the spiking region is larger than that of a single spiker but still drastically smaller than that of a tonic spiker. With this larger region, a ramp of duration 50 ms would cross through the spiking interval of applied current, so this short-duration, large-slope ramp would generate multiple spikes (Fig. 11A). Similar behavior is exhibited by single spiking neurons when exposed to a very short current ramp, as shown in Figure 12. For intermediate neurons, a ramp with a longer duration and smaller slope of, for example, 200 ms, would not pass through the spiking region. We would expect to see no spikes (Fig. 11B) or at most one spike with such a small-slope ramp (Fig. 11B). The one-parameter bifurcation structure for these two cases is shown in Fig. 11C for the large-slope ramp and Fig. 11D for the small-slope ramp. There is a large spiking interval for the large-slope ramp, but none for the small-slope ramp, explaining the time courses shown in Fig. 11A, B. These diagrams differ qualitatively from those of the single spiker (Fig. 8) and tonic spiker (Fig. 9), where tonic spiking intervals either did (tonic spiker) or did not (single spiker) exist for either ramp slope. Although we did not see intermediate neuron spiking patterns in our experimental studies of DA neurons, it would in principle be possible to see this from a spiking neuron with the titration of a channel blocker for the slowly-activated K⁺ current in the

cell, once the identity of that channel was determined, so that the whole-cell channel conductance is reduced but not entirely blocked.

4. Discussion

The goal of this study was to develop an analysis approach for understanding the response of a model neuron to fast applied current ramps. This topic arose from recent experimental work in which such ramps were employed in the characterization of the spiking properties of DA neurons of the rat OB (Korshunov et al., 2020). While bifurcation analysis using the applied current as the bifurcation parameter is desirable for such analysis, the existence of one or more variables that change on a relatively slow time scale make this problematic. We demonstrated how a decomposition of the model neuron into its fast and slow components could pave the way for employing bifurcation analysis on the fast subsystem, while constructing a functional relationship between the slow variable and the applied current to account for the slow subsystem. This provided the means of understanding the spiking behavior of the model neuron in response to fast ramps of different slopes, which parallel responses in actual DA neurons. This approach can be extended in a straight-forward manner to models with multiple slow variables.

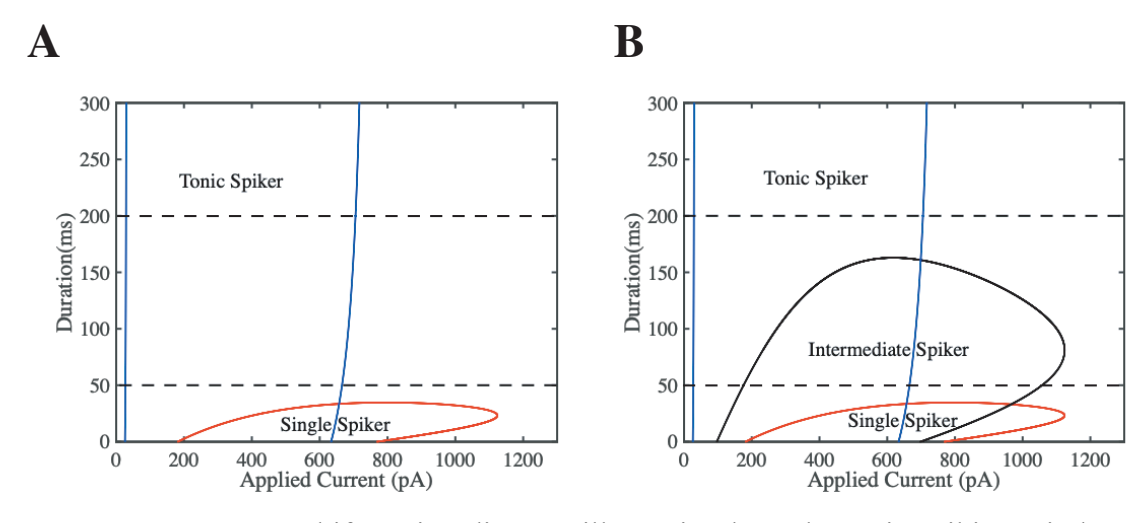


Fig. 10: Two-parameter bifurcation diagram illustrating how the tonic spiking window varies with ramp duration. In each case, the Hopf bifurcations in the one-parameter bifurcation diagram (Fig. 9) are traced out in a second parameter, the ramp duration. The model used includes equations (6), (7), and (16). (A) For the tonic spiker ($g_{KS} = 5 \text{ nS}$), the subcritical Hopf bifurcation branch (left blue curve) is nearly vertical, indicating that the initiation point of the tonic spiking behavior is relatively independent of the ramp duration (or slope). The termination point (right blue curve) increases with the ramp duration. The tonic spiking region is large, ensuring that ramps with a wide range of slopes will elicit tonic spiking behavior in these neurons. The dashed horizontal lines indicate the durations of the current ramps shown in earlier figures. The spiking region for the single spiker ($g_{KS} = 110 \text{ nS}$) (delimited by the red curve) is present only for short ramp durations. (B) The spiking region for a model neuron generated using $g_{KS} = 50 \text{ nS}$ has a spiking region that is intermediate between those that of the single spiker and that of the tonic spiker.

As shown in Fig. 10, the ramp speed can have a large impact on the fast-subsystem bifurcation diagram. Why does this happen? The answer lies in the fact that different ramp speeds change the cell's membrane potential at different rates; ramps with large slope increase V at a faster rate than small-slope ramps. This influences the activation variable z so that it increases at different rates for the different ramps. The result is a different fast-subsystem bifurcation diagram for different ramp slopes. As the ramp speed is reduced to low values the bifurcation diagram converges to that of the full system of equations.

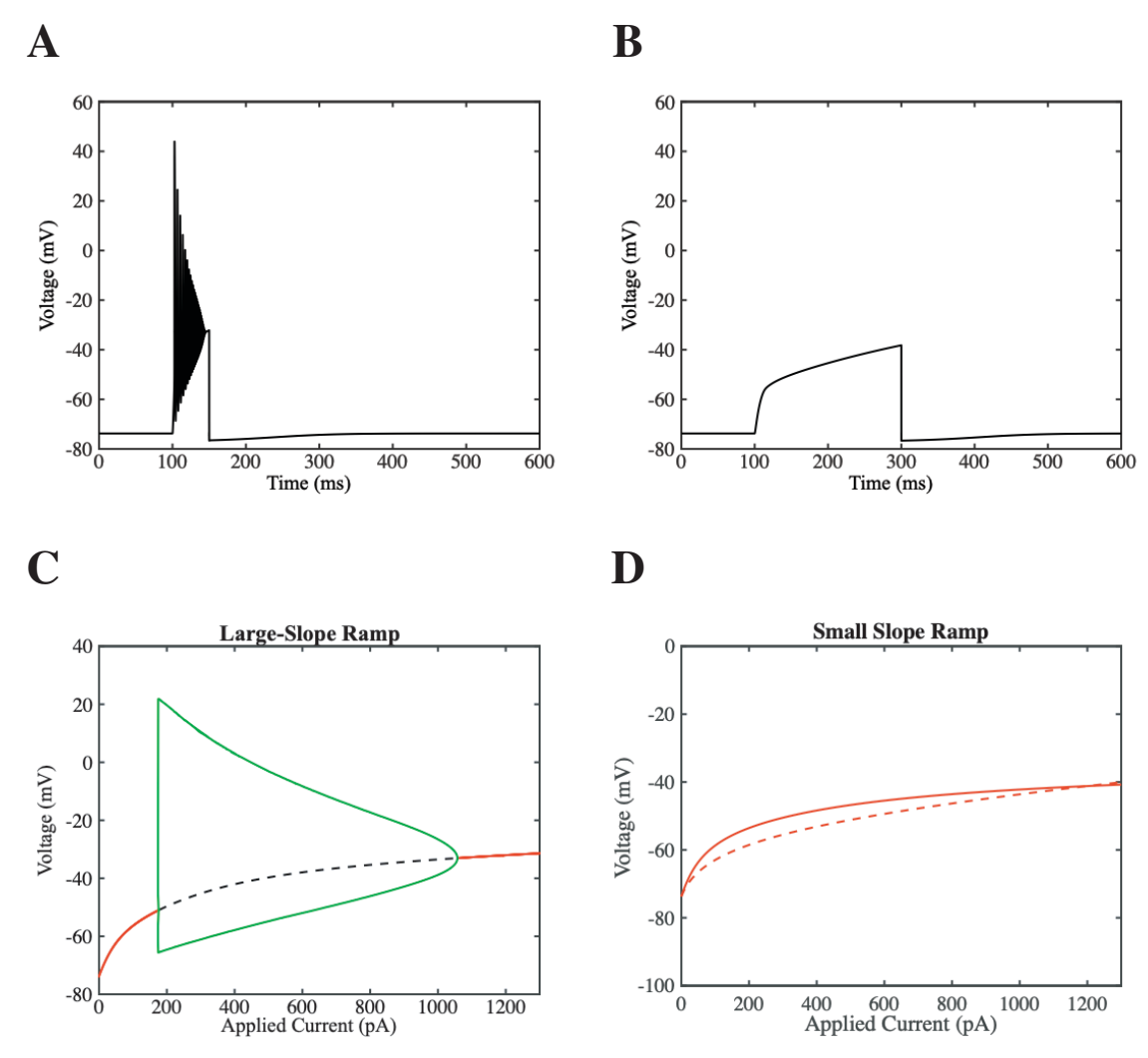


Fig. 11: Response of a model intermediate neuron ($g_{KS} = 50$ nS) to current ramps. (A) When the neuron is given an applied current ramp with a large slope (duration = 50 ms), it exhibits tonic spiking. (B) No spikes are produced during a small-slope current ramp (duration = 200 ms). (C) The bifurcation structure for the large-slope ramp has a large spiking interval. (D) There is no spiking interval for the small-slope ramp, as shown by the solid red line. This response is similar to that of an intermediate neuron when exposed to a slow ramp, which is shown with the dashed red line.

In addition to the mathematical analysis of fast ramps, we demonstrated how slow applied current ramps can be performed on biological neurons to provide information on the asymptotic spiking properties of the neuron (Fig. 4). We believe that such experimental bifurcation diagrams are useful for at least two reasons. First, they help in the partitioning of neurons into different "types" according to their asymptotic spiking properties. In the case studied here, a single-spiking neuron and a tonic spiker have very different asymptotic behavior, and this is readily revealed by the experimental bifurcation diagram produced with a slow current ramp. The second reason such diagrams are useful is that they help to constrain any mathematical model developed for the neuron; the model neuron should have the same qualitative asymptotic behavior as the neuron that is being modeled. Although only representative examples are shown in Fig. 4, we regularly found that single spiking neurons had a bifurcation structure similar to Fig. 4C (of the 11 recorded single spiking neurons, 9 did not show periodic branching in bifurcation diagrams), and tonic spikers had structure similar to Fig. 4D (of the 11 recorded tonic spiking neurons, 9 had periodic branching in bifurcation diagrams).

The model neuron that was used in this study was not calibrated to describe DA neurons. In fact, while our previous publication (Korshunov et al., 2020) did reveal differences in the activity of voltage-gated Na⁺ channels and the hyperpolarization-activated cyclic nucleotide (HCN) channel that produces the h-current, there was no attempt to fully elucidate the full mix of channels (e.g., K⁺ channels) present or to develop a biophysically accurate mathematical model of these neurons. It was not our aim, therefore, to make precise statements about these types of neurons. Instead, the aim was first to demonstrate that even a simple neuron model that captures the spiking behavior of a biological neuron subject to short current steps can convey useful information about the neuron's asymptotic behavior and its behavior in response to fast current ramps, and then to show how fast-slow analysis of the model neuron can bring insights about the spiking behavior of the neuron in response to fast current ramps. The analysis approach can be used with any single-compartment neural model, from simple (like ours) to much more complex models containing activation and inactivation variables for many ionic currents. Though implementation of the analysis would be more difficult with more complex models, the same basic approach should work.

Ionic current from a slowly activated K⁺ channel with a relatively large 50 ms time constant was a key element of our model. There are a number of ion channel types with slow gating properties. These include, but are not limited to, the activation of M-type K⁺ channels (Yue & Yaari, 2004), inactivation of A-type K⁺ channels (Connor & Stevens, 1971), activation of small (SK)-type and intermediate (IK)-type Ca²⁺-activated K⁺ channels (Kshatri et al., 2018), activation of ATP-sensitive K⁺ channels (Tinker et al., 2014), activation of the HCN-type channels (Wahl-Schott & Biel, 2009), and inactivation of L-type Ca²⁺ channels (Kubalova, 2003) and T-type Ca²⁺ channels (Perez-Reyes, 2003). All of these introduce slow components to the system, and depending upon the speed of the current ramp, some gating variables would be best grouped into the fast subsystem and some into the slow subsystem.

One big advantage that model neurons have over biological neurons is that the state of each gating variable is known at each point in time. Indeed, this knowledge is what allowed us to obtain the linear relationship between the slow gating variable and the applied current during a fast ramp. Although this can't be done for most gating variables in biological neurons, it is possible to do it for some. For example, activation of Ca²⁺-activated K⁺ channels is dependent on the intracellular free Ca²⁺ concentration, which can be measured using fluorescent dyes such as Fura-2 (Takahashi et al., 1999). Similarly, for ATP-sensitive K⁺ channels, the degree of activation is based on the ratio of ATP to ADP in the cell, and this can be determined with the fluorescent probe Perceval-

HR (Berg et al., 2009). Thus, in these instances, it would be possible to relate the activation factor to the applied current during a fast ramp, as we have done with the model neuron in this report. In so doing, a model neuron could be better calibrated to the physiology underlying the behavior of the biological neuron.

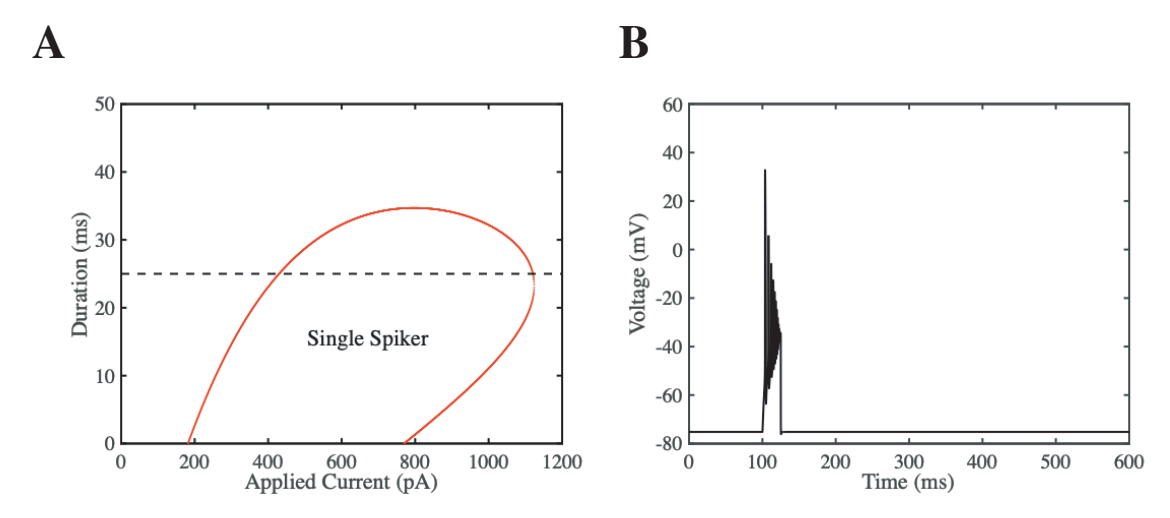


Fig. 12: Response of a single spiker neuron when exposed to a ramp with a short duration. (A) The two-parameter bifurcation diagram for a single spiking neuron. The dashed line for a ramp duration of 25 ms passes through two Hopf bifurcations, resulting in the spiking behavior shown in (B). This spiking behavior is similar to that of an intermediate neuron when exposed to a large-slope ramp, as shown in Fig. 11A.

Fast-slow analysis of models of excitable cells has been used to understand a range of behaviors, including bursting oscillations (Bertram & Rubin, 2017; Izhikevich, 2000), pathological fluctuations in the membrane potential of cardiac myocytes (Kimrey et al., 2020a; Kügler, 2016), and oscillations in the intracellular Ca²⁺ concentration (Harvey et al., 2011). In each instance, the objective was to go beyond computer simulations as a means for characterizing the behavior of the model cell. That is, to not just demonstrate what can happen, but to understand why it happens. We see the application of fast-slow analysis to neural spiking during current ramps in the same light.

5. Acknowledgements

We thank Dr. Laura Blakemore for her careful reading of the manuscript and helpful comments, and Dr. Theodore Vo for initial discussions. This work was supported by the FSU Chemosensory Training Program (CTP) Grant Award T32 DC000044 from the National Institutes of Health (NIH/NIDCD), NIH Grant R21DA044442 to PQT and RB, and grant number DMS 1853342 from the National Science Foundation to RB.

6. References

Berg, J., Hung, Y. P., & Yellen, G. (2009). A genetically encoded fluorescent reporter of ATP: ADP ratio. *Nature Methods*, 6(2), 161-166.

- Bertram, R., & Rubin, J. E. (2017). Multi-timescale systems and fast-slow analysis. *Mathematical Biosciences*, 287, 105-121.
- Carroll, B. J., Bertram, R., & Hyson, R. L. (2018). Intrinsic physiology of inhibitory neurons changes over auditory development. *Journal of Neurophysiology*, *119*(1), 290-304.
- Connor, J., & Stevens, C. (1971). Voltage clamp studies of a transient outward membrane current in gastropod neural somata. *The Journal of Physiology*, 213(1), 21-30.
- Cury, K. M., & Uchida, N. (2010). Robust odor coding via inhalation-coupled transient activity in the mammalian olfactory bulb. *Neuron*, 68(3), 570-585.
- Daou, A., Ross, M. T., Johnson, F., Hyson, R. L., & Bertram, R. (2013). Electrophysiological characterization and computational models of HVC neurons in the zebra finch. *Journal of Neurophysiology*, 110(5), 1227-1245.
- Desroches, M., Guckenheimer, J., Krauskopf, B., Kuehn, C., Osinga, H. M., & Wechselberger, M. (2012). Mixed-mode oscillations with multiple time scales. *SIAM Review*, *54*(2), 211-288.
- Dovzhenok, A., & Kuznetsov, A. S. (2012). Exploring neuronal bistability at the depolarization block. *PLoS ONE*, 7(8), e42811.
- Golomb, D., Yue, C., & Yaari, Y. (2006). Contribution of persistent Na⁺ current and M-type K⁺ current to somatic bursting in CA1 pyramidal cells: combined experimental and modeling study. *Journal of Neurophysiology*, *96*(4), 1912-1926.
- Harvey, E., Kirk, V., Wechselberger, M., & Sneyd, J. (2011). Multiple timescales, mixed mode oscillations and canards in models of intracellular calcium dynamics. *Journal of Nonlinear Science*, 21(5), 639-683.
- Hasan, C. R., Krauskopf, B., & Osinga, H. M. (2018). Saddle Slow Manifolds and Canard Orbits in R⁴ and Application to the Full Hodgkin–Huxley Model. *The Journal of Mathematical Neuroscience*, 8(1), 1-48.
- Iacovitti, L., Wei, X., Cai, J., Kostuk, E. W., Lin, R., Gorodinsky, A., Roman, P., Kusek, G., Das, S. S., & Dufour, A. (2014). The hTH-GFP reporter rat model for the study of Parkinson's disease. *PloS ONE*, *9*(12), e113151.
- Izhikevich, E. M. (2000). Neural excitability, spiking and bursting. *International Journal of Bifurcation and Chaos*, 10(06), 1171-1266.
- Kimrey, J., Vo, T., & Bertram, R. (2020a). Big Ducks in the Heart: Canard Analysis Can Explain Large Early Afterdepolarizations in Cardiomyocytes. *SIAM Journal on Applied Dynamical Systems*, 19(3), 1701-1735.

- Kimrey, J., Vo, T., & Bertram, R. (2020b). Canard analysis reveals why a large Ca²⁻ window current promotes early afterdepolarizations in cardiac myocytes. *PloS Computational Biology*, *16*(11), e1008341.
- Korshunov, K. S., Blakemore, L. J., Bertram, R., & Trombley, P. Q. (2020). Spiking and membrane properties of rat olfactory bulb dopamine neurons. *Frontiers in Cellular Neuroscience*, 14, 60.
- Kshatri, A. S., Gonzalez-Hernandez, A., & Giraldez, T. (2018). Physiological roles and therapeutic potential of Ca²⁺ activated potassium channels in the nervous system. *Frontiers in Molecular Neuroscience*, 11, 258.
- Kubalova, Z. (2003). Inactivation of L-type calcium channels in cardiomyocytes. Experimental and theoretical approaches. *General Physiology and Biophysics*, 22(4), 441-454.
- Kügler, P. (2016). Early afterdepolarizations with growing amplitudes via delayed subcritical Hopf bifurcations and unstable manifolds of saddle foci in cardiac action potential dynamics. *PloS ONE*, 11(3), e0151178.
- Lübke, J., Frotscher, M., & Spruston, N. (1998). Specialized electrophysiological properties of anatomically identified neurons in the hilar region of the rat fascia dentata. *Journal of Neurophysiology*, 79(3), 1518-1534.
- Perez-Reyes, E. (2003). Molecular physiology of low-voltage-activated t-type calcium channels. *Physiological Reviews*, 83(1), 117-161.
- Ross, M. T., Flores, D., Bertram, R., Johnson, F., Wu, W., & Hyson, R. L. (2019). Experience-dependent intrinsic plasticity during auditory learning. *Journal of Neuroscience*, 39(7), 1206-1221.
- Rubin, J., & Wechselberger, M. (2007). Giant squid-hidden canard: the 3D geometry of the Hodgkin–Huxley model. *Biological Cybernetics*, 97(1), 5-32.
- Sherman, A. (2011). Dynamical systems theory in physiology. *Journal of General Physiology*, 138(1), 13-19.
- Takahashi, A., Camacho, P., Lechleiter, J. D., & Herman, B. (1999). Measurement of intracellular calcium. *Physiological Reviews*, 79(4), 1089-1125.
- Tinker, A., Aziz, Q., & Thomas, A. (2014). The role of ATP-sensitive potassium channels in cellular function and protection in the cardiovascular system. *British Journal of Pharmacology*, *171*(1), 12-23.
- Vo, T., Bertram, R., & Wechselberger, M. (2013). Multiple geometric viewpoints of mixed mode dynamics associated with pseudo-plateau bursting. *SIAM Journal on Applied Dynamical Systems*, 12(2), 789-830.

- Wahl-Schott, C., & Biel, M. (2009). HCN channels: structure, cellular regulation and physiological function. *Cellular and Molecular Life Sciences*, 66(3), 470-494.
- Yue, C., & Yaari, Y. (2004). KCNQ/M channels control spike afterdepolarization and burst generation in hippocampal neurons. *Journal of Neuroscience*, 24(19), 4614-4624.